

Tungsten Disulphide Sheathed Carbon Nanotubes

Raymond L. D. Whitby,^[a] Wen Kuang Hsu,^[a]
Chris B. Boothroyd,^[b] Peter K. Fearon,^[a]
Harold W. Kroto,^[a] and David R. M. Walton^{*[a]}

KEYWORDS:

carbon · electron diffraction · layered compounds · nanotubes · tungsten disulphide

Tenne et al. pioneered the nanotechnology of inorganic fullerene particles and nanotubes.^[1] An inherent aspect of producing MX_2 nanotubes ($M = \text{W}$ or Mo , $X = \text{S}$ or Se) is that their dimensions are essentially determined by the morphology of metal oxide precursors, namely the template effect.^[2] This creates a difficulty in the formation of single-walled MX_2 nanotubes, as the smallest oxide particles (5 nm in diameter)^[3] will result in at least three-layered WS_2 nanotubes, where the smallest inner core diameter would be about 0.4–1.2 nm with a 6.2 Å d-spacing.^[4] As a consequence, the band theory of a hollow single-walled MX_2 nanotube, based on the rolling up of an MX_2 sheet,^[5] cannot be tested experimentally. Herein we report the successful production of single- and double-layered WS_2 -coated multiwalled carbon nanotubes (MWCNs) by pyrolysing $\text{H}_2\text{S}/\text{N}_2$ over WO_3 -coated MWCNs at 900 °C. The single-layered WS_2 -coated MWCNs in particular provide an opportunity for I - V measurement using the photolithography technique^[6] and for local density of states (LDOS) probe by STM.^[7]

The formation of WS_2 -coated MWCNs implies that WO_3 is converted into WS_2 directly on the MWCN surfaces. The first step towards this goal is to deposit WO_3 on MWCNs. However, the wetting of MWCNs is difficult, due to high surface tension.^[8] Preliminary attempts involved oxidation of MWCNs prior to the oxide coating process. However, this method causes significant damage to the MWCN surface and the yield of coated materials is very low.^[9] In this present work we have avoided damaging the surface of MWCNs.

Prior to the H_2S pyrolysis, high-resolution transmission microscopy (HRTEM) revealed that the 350 °C heat-treated mixture of MWCNs and H_2WO_4 contained MWCNs coated with an amorphous layer, which was 0.5–2 nm thick. Energy-dispersive X-ray microanalysis (EDX) showed the presence of carbon, tungsten and oxygen. The carbon signal arises from the MWCNs and the amorphous coating is WO_{3-x} ($x = 0-1$).

HRTEM showed that 60% of the MWCNs were either fully or partly coated with dark material, typically with one to three layers. The polyhedral carbon particles were also partly coated. Figure 1 shows two typical MWCNs coated with a) a single-layer and b) a double-layer of WS_2 . EDX analyses (50 s lifetime, 110–120 K spec-

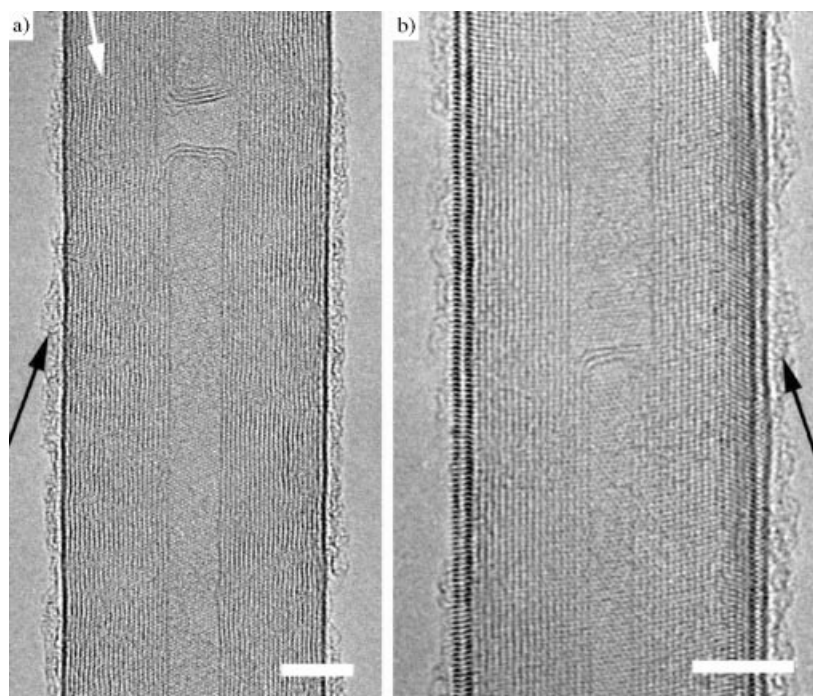


Figure 1. HRTEM images of a MWCN coated with a) single and b) double layer of WS_2 . Scale bars = 5 nm.

trum counts) were carried out on both partly and fully coated MWCNs. Only a carbon signal was present when the EDX probe was focused on the uncoated section of a partly coated MWCN. When the probe was focused on the coated area, carbon, tungsten and sulfur, together with a trace of oxygen, were detected (Figure 2). Carbon, tungsten and sulfur were always present when the EDX probe was focused on a fully coated MWCN. Small quantities of oxygen were occasionally detected in fully coated MWCNs. The atomic ratio of tungsten to sulfur was about $1:2 \pm 0.1$ (that is, WS_2). It is clear from HRTEM and EDX that the coating material is WS_2 and that the carbon signal arises from the MWCNs. This conclusion is also supported by X-ray linescans, which revealed that the MWCNs were actually sheathed within WS_2 .

Several features are distinguishable, based on Figure 1: a) the graphite layered structure (spacing 3.4 Å) of the MWCN is maintained after H_2S pyrolysis; b) the d-spacing of the double-layer WS_2 coating (Figure 1 b) is about 6.2 Å, consistent with expected separation;^[3-4] c) the WS_2 layers exhibit basal plane

[a] Dr. D. R. M. Walton, R. L. D. Whitby, Dr. W. K. Hsu, P. K. Fearon, Prof. H. W. Kroto
School of Chemistry, Physics and Environmental Science
University of Sussex
Brighton, BN1 9QJ (UK)
Fax: (+44) 1273-877766
E-mail: d.walton@sussex.ac.uk

[b] Dr. C. B. Boothroyd
Department of Materials Science and Metallurgy
University of Cambridge
Cambridge, CB2 3QZ (UK)

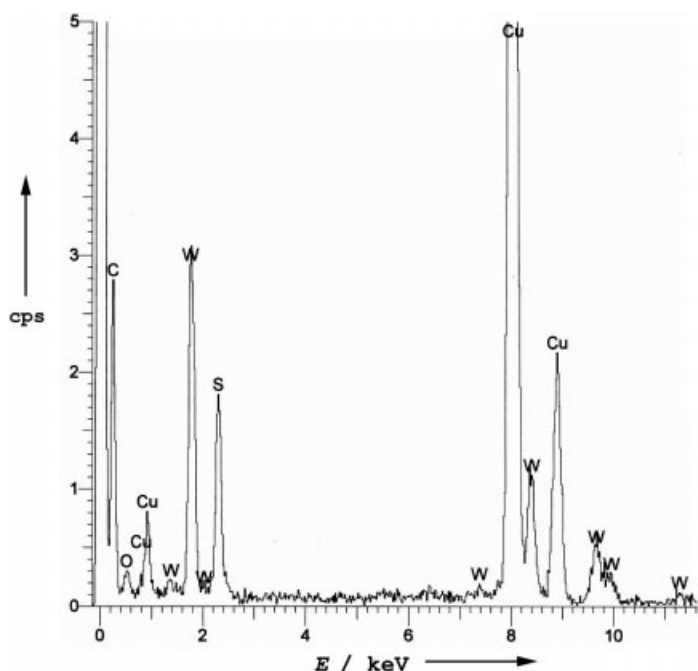


Figure 2. EDX spectrum of a WS_2 -coated MWCN. The copper signal arises from the TEM grid.

lattice fringes which are darker than the carbon layers; d) the WS_2 layers are parallel to the MWCN basal planes; e) the distance between the centre of the WS_2 layer to the centre of the outermost carbon layer is around 4.4 \AA ; f) the residual amorphous WO_{3-x} (dark arrows in Figure 1), due to incomplete $WO_3 \rightarrow WS_2$ conversion, is present on the coated surfaces; g) striation patterns, derived from the WS_2 coating, are present (white arrows in Figure 1).

An electron diffraction pattern obtained from a double layer WS_2 -coated MWCN is shown in Figure 3. The difficulty lies in analysing diffraction patterns arising from the overlap of WS_2 and MWCN spot arrays. We can consider the WS_2 and MWCN diffraction spots separately. The front and back WS_2 layers of the tube will produce two $[0001]$ WS_2 diffraction patterns superimposed on one another. The tube is helical and shows the WS_2 pattern inclined by 9° with respect to the tube axis. The $\{10\bar{1}0\}$ spots (spacing 2.73 \AA) of the front and back patterns are indexed with and without parentheses in Figure 3. It is not possible to tell which is the front and which is the back without knowing the direction of the tube helix. One of these faces (indexed in parentheses) is much fainter than the other. This suggests that the WS_2 probably does not cover both surfaces of the tube evenly, but has a greater number of layers on one surface. The side walls of the WS_2 coating are only two layers thick and, hence, produce a 0002 streak rather than a discrete spot. The parts of the WS_2 coating between the front and the sides give rise to the streaking of the $\{10\bar{1}0\}$ spots. The MWCN generates a set of diffraction spots similar to the WS_2 layers, however the spacings are larger on the diffraction pattern owing to the smaller graphite lattice spacing. It is difficult to distinguish between many of the graphite $[0001]$ reflections from the front

and rear surfaces of the tube; possibly because this tube has a number of different helix angles throughout its thickness. The 0002 spots from the side walls are easily visible and are indexed on Figure 3.

Previous reports showed that the MWCNs are significantly damaged when heated at $700\text{--}750^\circ\text{C}$ for 30 min and lose about 99% mass.^[10] We find that the WS_2 coating is capable of acting as an antioxidant for MWCNs. By way of comparison, three samples—A) arc-generated MWCNs; B) WS_2 nanostructures, including nanotubes and particles, prepared by pyrolysing H_2S over WO_3 precursor at 950°C as described previously;^[11a–b] C) WS_2 -coated MWCNs—were heated in air to 950°C within a thermogravimeter (Perkin Elmer, TGA7, 10 Kmin^{-1}). The results are shown in Figure 4.

- A) MWCNs, red line: Oxidation begins at about 700°C , and drastic mass loss occurs between $700\text{--}900^\circ\text{C}$. At around 910°C , the mass loss of MWCNs is approximately 99%. The TGA profile of MWCNs is consistent with previous results;^[10]
- B) WS_2 nanostructures, green line: A 3.4% mass loss occurs at around 530°C , which is attributed to WS_2 conversion into WO_3 , resulting in a light-green powder. No further mass loss occurs between $500\text{--}950^\circ\text{C}$;
- C) WS_2 -coated MWCNs, purple line: A stepwise profile is observed. The first mass loss begins at 450°C , attributed to the onset of WS_2 coating $\rightarrow WO_3$ conversion. Between $450\text{--}550^\circ\text{C}$, the mass loss is approximately 8%. A minor mass loss (2%) occurs between $550\text{--}700^\circ\text{C}$. From 700 to 830°C , the mass loss is around 30%, and no further mass loss is recorded above 830°C .

The dark-green residue resulting from the oxidation of WS_2 -coated MWCNs was subsequently analysed by TEM and EDX.

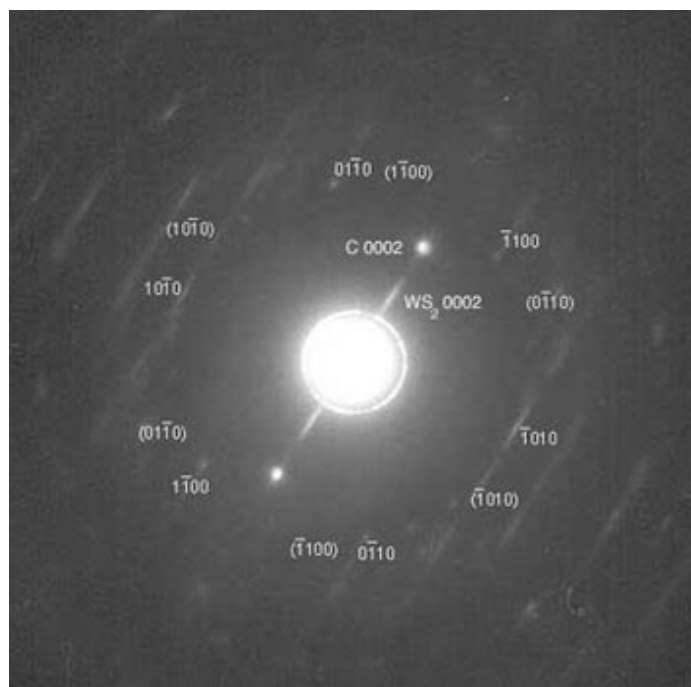


Figure 3. An indexed electron diffraction pattern of a double-layer WS_2 -coated MWCN. The $\{10\bar{1}0\}$ diffraction spots from the front and rear WS_2 surfaces are indexed (indices from one surface are in parentheses), as are the 0002 spots from the WS_2 (WS_2 0002) and from the carbon nanotube (C 0002).

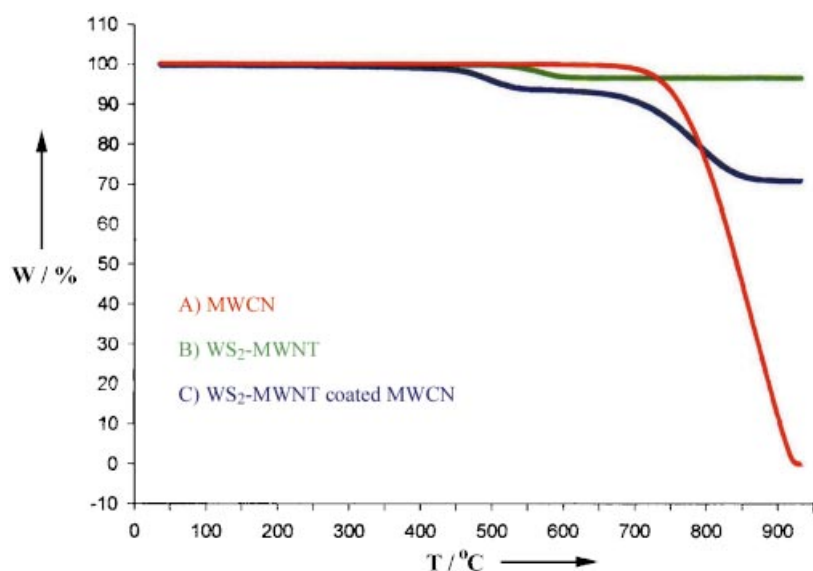


Figure 4. Thermogravimetric analysis of MWCNs, WS_2 nanostructures and WS_2 -coated MWCNs.

TEM revealed the presence of MWCNs and particles, where MWCNs exhibit minimal surface damage and are uncapped (Figure 5a). The oxidation of MWCNs results in tapered tubes

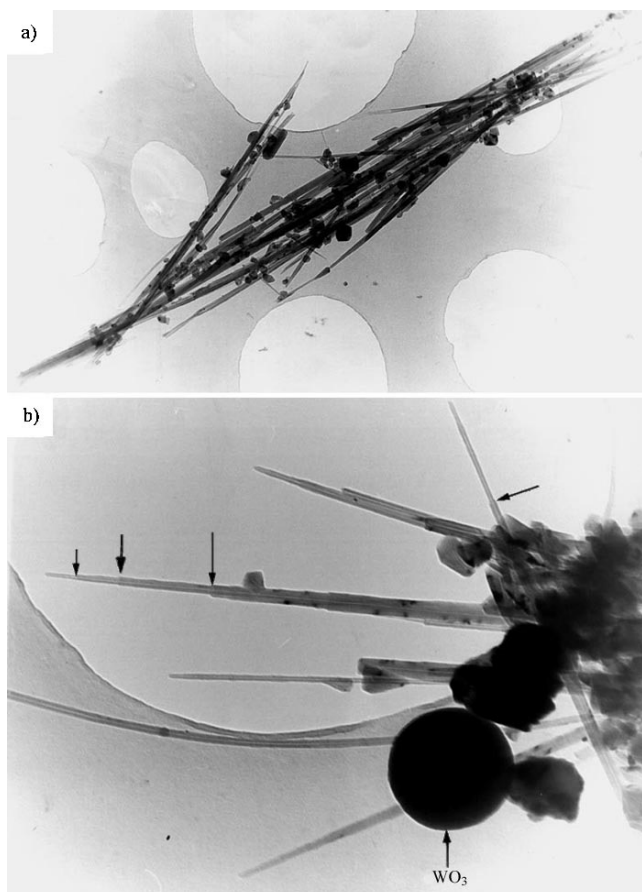


Figure 5. TEM images of a) WS_2 -coated MWCNs after TGA and b) oxidised MWCNs and the end product of WS_2 particles converted into WO_3 (arrow) after TGA. Selected MWCNs exhibit a reduction in the number of carbon layers towards the tube tip, due to peeling.

(arrows, Figure 5b) due to peeling. TEM also revealed the presence of a very thin amorphous coating (< 1 nm thick) on MWCN surfaces, possibly consisting of WO_3 . Larger WO_3 particles, possibly originating from the initial oxidation prior to H_2S pyrolysis, are also present (Figure 5b). EDX of oxidized MWCNs revealed the presence of tungsten, carbon and oxygen; sulfur was absent. According to TEM and EDX analyses, the WS_2 coating has delayed the oxidation of MWCNs and particles via $WS_2 \rightarrow WO_{3-x}$ conversion. First, when the temperature reaches $450^\circ C$, the WS_2 coating begins to convert into WO_3 (Figure 4, purple line). A similar process applies to WS_2 nanostructures (Figure 4, green line), however the conversion begins around $80^\circ C$ lower than in the case of WS_2 nanostructures ($530^\circ C$). This may be attributed to the more defective thinner deposition of WS_2 layers on the MWCNs and would allow easier diffusion of oxygen, thereby leading to accelerated conversion.

At $600-700^\circ C$, the uncoated MWCNs and particles (30–40% overall) begin to oxidize, a process which accelerates when the temperature is raised to about $830^\circ C$. Meanwhile the WS_2 coatings are continuously converted into WO_{3-x} .^[12a-b] At $900^\circ C$, the uncoated MWCNs and particles have been fully oxidized and the $WS_2 \rightarrow WO_{3-x}$ conversion is complete. The WO_{3-x} ($x = 0-1$) thus formed, subsequently sublimates at around $900-950^\circ C$,^[12a-b] which accounts for the presence of a very thin WO_{3-x} coating on MWCNs. The onset of oxidation of MWCNs partly coated with WS_2 should occur at a slightly higher temperature than that for uncoated MWCNs, possibly in the range $800-900^\circ C$.

In summary, it was shown previously that MWCNs could be utilized as templates for the deposition of metal oxides.^[13] In this paper we have demonstrated that carbon nanotubes can provide a support for topological reactions without damaging the template and that WS_2 coating confers oxidative stability on the MWCNs by undergoing sacrificial oxidation to WO_{3-x} .

Experimental Section

Tungstic acid (250 mg) and arc-generated MWCNs (50 mg) were added to liquid ammonia at $-78^\circ C$ and the mixture was allowed to attain room temperature. The solid residue was then heated to $350^\circ C$ for 30 min in an air stream ($100\text{ cm}^3\text{ min}^{-1}$) in order to convert tungstic acid into tungsten oxide, and then at $900^\circ C$ in N_2/H_2S (3/1 ratio, $50\text{ cm}^3\text{ min}^{-1}$ total flow rate) for 10 min. The resulting black product was subjected to HRTEM (JEOL 4000-EXII), EDX and electron diffraction analysis.

We thank the Leverhulme Trust, the Royal Society and the EPSRC (UK) for financial support. We are also grateful to D. Randall and J. Thorpe (University of Sussex) for assistance with TEM analysis, and N. Billingham (University of Sussex) for TGA discussions.

- [1] R. Tenne, L. Margulis, M. Genut, G. Hodes, *Nature* **1992**, *360*, 444–446.
 [2] Y. Feldman, G. Frey, M. Homyonfer, V. Lyakhovitskaya, L. Margulis, H. Cohen, G. Hodes, J. Hutchison, R. Tenne, *J. Am. Chem. Soc.* **1996**, *118*, 5362–5367.
 [3] M. Hershinkel, L. Gheber, V. Volterra, J. Hutchison, L. Margulis, R. Tenne, *J. Am. Chem. Soc.* **1994**, *116*, 1914–1917.
 [4] N. Wang, Z. K. Tang, G. D. Li, J. S. Chen, *Nature* **2000**, *408*, 50–51.
 [5] G. Seifert, H. Terrones, M. Terrones, G. Jungnickel, T. Frauenheim, *Phys. Rev. Lett.* **2000**, *85*, 146–149.
 [6] T. W. Ebbesen, H. J. Lezec, H. Hiura, J. W. Bennett, H. F. Ghaemi, T. Thio, *Nature* **1996**, *382*, 54–56.
 [7] D. L. Carroll, P. Redlich, X. Blase, J.-C. Charlier, S. Curran, P. M. Ajayan, S. Roth, M. Rühle, *Phys. Rev. Lett.* **1998**, *81*, 2332–2335.
 [8] E. Dujardin, T. W. Ebbesen, H. Hiura, K. Tanigaki, *Science* **1994**, *265*, 1850–1852.
 [9] W. K. Hsu, Y. Q. Zhu, H. W. Kroto, D. R. M. Walton, R. Kamalakaram, M. Terrones, *Appl. Phys. Lett.* **2000**, *77*, 4130–4132.
 [10] T. W. Ebbesen, P. M. Ajayan, H. Hiura, K. Tanigaki, *Nature* **1994**, *367*, 519.
 [11] a) Y. Q. Zhu, W. K. Hsu, H. Terrones, N. Grobert, B. H. Chang, M. Terrones, B. Q. Wei, H. W. Kroto, D. R. M. Walton, C. B. Boothroyd, I. Kinloch, G. Z. Chen, A. H. Windle, D. J. Fray, *J. Mater. Chem.* **2000**, *10*, 2570–2577; b) W. K. Hsu, Y. Q. Zhu, S. Firth, M. Terrones, H. Terrones, S. Trasobares, R. J. H. Clark, H. W. Kroto, D. R. M. Walton, *Carbon* **2001**, *39*, 1107–1111.
 [12] a) W. B. Hu, Y. Q. Zhu, W. K. Hsu, B. H. Chang, M. Terrones, N. Grobert, H. Terrones, J. P. Hare, H. W. Kroto, D. R. M. Walton, *Appl. Phys. A* **2000**, *70*, 231–233; b) Y. Q. Zhu, W. B. Hu, W. K. Hsu, M. Terrones, N. Grobert, J. P. Hare, H. Terrones, H. W. Kroto, D. R. M. Walton, *Chem. Phys. Lett.* **1999**, *309*, 327–334.
 [13] B. C. Satishkumar, A. Govindaraj, M. Math, C. N. R. Rao, *J. Mater. Chem.* **2000**, *10*, 2115–2119.

Received: July 13, 2001 [Z260]

Design of Biofunctional Assemblies on Solids through Recombinant Spherical Bacterial Protein Lumazine Synthase

Markus Fischer,^[b] Adelbert Bacher,^[b] Ilka Haase,^[b] Matthias Tristl,^[a] and Erich Sackmann^{*[a]}

KEYWORDS:

actin cortex modeling · interfaces · lumazine synthase · phospholipids · supported membranes

The interest in microstructured biofunctional surfaces has increased dramatically during the last few years owing to numerous potential practical and scientific applications.

[a] Prof. Dr. E. Sackmann, M. Tristl
 Physik Department
 Technische Universität München
 James Franck Strasse, 85748 Garching (Germany)
 E-mail: sackmann@ph.tum.de

[b] Dr. M. Fischer, Prof. Dr. A. Bacher, I. Haase
 Lehrstuhl für Organische Chemie und Biochemie
 Technische Universität München
 Lichtenbergstrasse 4, 85748 Garching (Germany)

Practical perspectives include

- the design of smart biosensors on electro-optical devices,^[1–3] and
- the surface anchoring of proteins under non-denaturing conditions for example for applications in the rapidly developing field of proteomics or to stimulate tissue growth on transplants.^[4]

Scientific applications include

- studies of the physical basis of self-assembly of biomembranes and lipid/protein interaction mechanisms by various surface sensitive techniques, and
- the design of mimetics of cell and tissue surfaces to study the regulation of cell adhesion by the interplay of receptor mediated lock-and-key forces, universal interfacial forces, and the cell membrane elasticity.^[5]

For all applications it is important to separate the biofunctional entities (for example cells) from the denaturing inorganic solids (which may be toxic, such as devices based on GaAs semiconductors) by ultrathin biocompatible films. Biocompatible polar films have been formed by the surface grafting of ultrathin hydrophilic polymer films composed of synthetic polymer dextran (as used in surface plasmon resonance devices), hyaluronic acid,^[6] or by the deposition of multilayers of cellulose.^[7] Another successful strategy to functionalize solids is to deposit fluid, self-healing membranes.^[8] This is achieved by separation of the membrane and the solid by ultrathin soft polymer cushions such as lipopolymers,^[9] hairy rod multilayers,^[7] or by monolayers of glycoproteins of the outer cell wall of bacteria, so called S-layers.^[10]

Supported membranes exhibit several advantages. The density and mobility of functional groups (such as receptors) can be controlled. Functional patterns can be generated by making use of lateral phase separation^[11] and the lateral organization of the components can be manipulated by two-dimensional electrophoresis.^[12, 13]

In the present work we introduce a versatile new tool for the design of smart biomimetic solid surfaces based on recombinant lumazine synthase (LuSy) from *Bacillus subtilis*. Lumazine synthases can exist in a number of different oligomerization states. Lumazine synthases from *Brucella abortus*,^[14] yeast,^[15] and certain fungi^[16] are homopentamers. Icosahedral structures with 60 subunits (triangulation number $T=1$) are formed by lumazine synthases of spinach,^[16] *B. subtilis*^[17] (Figure 1), and *Aquifex aeo-*

Abbreviations:

ATP	adenosine-5'-triphosphate
DDT	1,4-dithio threitol
DOGS-NTA-Ni	1,2-dioleoyl- <i>sn</i> -glycero-3-[N-(5-amino-1-carboxypentyl)iminodiacetic acid)succinyl] (nickel salt)
DMPC	dimyristoylphosphatidylcholine
DHPE-TR	N-(Texas red sulfonyl)-1,2-dihexadecanoyl- <i>sn</i> -glycero-3-phosphoethanolamine
EDTA	ethylenediaminetetraacetate
IPTG	isopropyl- β -D-thiogalactopyranoside
LuSy	lumazine synthase
NTA	nitrilotriacetic acid
SDS	sodium dodecyl sulfate
Tris	tris(hydroxymethyl)aminomethane